https://doi.org/10.1038/s44306-025-00105-z

Deterministic spin-orbit torque switching of epitaxial ferrimagnetic insulator with perpendicular magnetic anisotropy fabricated by on-axis magnetron sputtering

Roselle Ngaloy[1,7], Naoto Yamashita[1,2,7] ✉, Bing Zhao[1], Soojung Kim[3], Kohei Yamashita[4], Ivo P. C. Cools[1], Marlis N. Agusutrisno[4,5], Soobeom Lee[3,6], Yuichiro Kurokawa[2], Chun-Yeol You[3], Hiromi Yuasa[2] & Saroj P. Dash[1] ✉

Current-induced switching of magnetization states in ferromagnet/spin-orbit material heterostructures has attracted significant attention, driven by the increasing need for low power consumption and a more efficient mechanism for magnetization switching. However, current shunting for the used metallic ferromagnets remains challenging in achieving low switching current densities. Thulium iron garnet, $Tm_3Fe_5O_{12}$ (TmIG), is promising for such devices as it exhibits strong perpendicular magnetic anisotropy (PMA) and fast magnetization dynamics. However, there still remains a technological challenge in the growth of TmIG films using industry-compatible magnetron sputtering in a simple on-axis geometry for spintronic device applications. Here, we demonstrated the spin-orbit torque (SOT) magnetization switching of TmIG thin film grown by on-axis radio-frequency magnetron sputtering. Robust and deterministic SOT magnetization switching is achieved using TmIG/Pt heterostructures at a current density as low as 0.7×10^{11} A/m^2. Anomalous Hall and second harmonic Hall measurements were performed to quantify effective spin-orbit fields. The effective field inducing damping-like torque is estimated to be 21±1 Oe per 10^7 A/cm^2, higher than previous reports. These findings show a growth method for ferrimagnetic insulators with strong PMA in industry-compatible on-axis sputtering methods and its utilization for achieving energy-efficient SOT non-volatile memory applications.

In recent years, current-induced magnetization switching via spin-orbit torque (SOT) has attracted a lot of attention to realize non-volatile, energy-efficient, and faster magnetic random-access memory (MRAM) and domain-wall magnetic racetrack memory[1–3]. A fascinating SOT material system is a combination of a perpendicularly magnetized ferrimagnetic insulator, thulium iron garnet ($Tm_3Fe_5O_{13}$, TmIG), and a large spin Hall conductivity metal, platinum (Pt)[4,5]. The strong perpendicular magnetic anisotropy (PMA) in epitaxially grown TmIG thin films stems from the strain in the film[6] due to the lattice mismatch with the gadolinium gallium garnet ($Ga_3Gd_5O_{12}$, GGG) substrate. TmIG has a negatively large magneto-

[1]Department of Microtechnology and Nanoscience, Chalmers University of Technology, Gothenburg, SE-41296, Sweden. [2]Faculty of Information Science and Electronics Engineering, Kyushu University, 744 Motooka Nishiku Fukuoka, Fukuoka, 819-0379, Japan. [3]Department of Physics and Chemistry, DGIST, Techno Jungang-daero 333, Hyeonpung-myeon, Dalseong-gun, Daegu, 42988, South Korea. [4]Graduate School of Information Science and Electronics Engineering, Kyushu University, 744 Motooka Nishiku Fukuoka, Fukuoka, 819-0379, Japan. [5]Department of Electrical Engineering, Sultan Ageng Tirtayasa University, 42435 Banten, Indonesia. [6]Department of Electrical and Computer Engineering, Shinshu University, Nagano, 380-0928, Japan. [7]These authors contributed equally: Roselle Ngaloy, Naoto Yamashita. ✉e-mail: yamashita.naoto.952@m.kyushu-u.ac.jp; saroj.dash@chalmers.se

elastic constant ($\lambda_{111} = -5.2 \times 10^{-6}$) and moderate lattice constant mismatch with GGG substrate (0.49%)[6,7]. The sizable Dzyaloshinskii-Moriya Interaction (DMI) is also beneficial for the spin-orbitronic device applications[8–11].

Although TmIG is an insulator, its magnetization can be electrically detected by fabricating a heterostructure with non-magnetic metals like Pt[12–18]. The interfacial proximity-induced effects have been gathering interest due to their application potential for SOT memory devices[19–22]. After the first demonstration of the SOT-switching in TmIG[23], TmIG/Pt systems were intensively pursued to address the necessity of spin-based memory and logic devices[24–31], as well as recent studies using orbital torque effects[32,33]. The intrinsic nature of the observed field-free magnetization switching in TmIG/Pt is of particular interest, as Ke et al. observed three-fold symmetry in the critical current density[28], whilst Husain et al. observed four-fold symmetry[29]. Three-fold symmetry is attributed to the intrinsic nature of the TmIG crystal, whilst the source of the four-fold symmetry is still unclear. Therefore, a better understanding of the growth methods of TmIG, their symmetry, and the physics behind the spin-orbit torque current-induced magnetization switching is important for energy-efficient spintronic devices.

Industry-compatible fabrication technologies for new materials are essential for connecting fundamental science with practical device applications. TmIG emerged in modern spintronics in 2012, where the thin films were grown using pulse laser deposition (PLD)[6] and subsequently SOT magnetization switching has also been demonstrated in 2017[5,23]. Since then, most of the experimental work has been reported using PLD growth techniques and some reports using the sputtering deposition technique using a unique off-axis geometry[4–13,16,18,23–33]. Off-axis sputtering benefits to reduce the plasma damage on the film and fabricating SOT devices with a non-magnetic metallic film. The geometries of off-axis and on-axis sputtering (Fig. 1a, b), play a critical role in this process. In off-axis sputtering, the substrates are positioned outside the flux's axis, whereas in on-axis sputtering, the substrates are placed around the flux's axis[34,35]. A benefit of on-axis sputtering compared with off-axis sputtering is increased productivity, where the size of the film is not limited by the geometry of the deposition system but only by the size of the target, and hence is preferred mostly by industry. Another major difference between on-axis sputtering and other techniques (off-axis sputtering and laser ablation) is exposure to anion irradiation during deposition. However, using the on-axis sputtering technique, the SOT switching of the TmIG/Pt has not been examined yet[34,35].

In this study, we show a high-quality crystalline TmIG fabricated by *on-axis* radio frequency (RF)-magnetron sputtering and demonstrate robust SOT magnetization switching at room temperature. We optimized the growth atmosphere, such as the O_2 flow rate, during the deposition of TmIG. Utilizing such TmIG films and their heterostructures with Pt, we performed deterministic SOT magnetization switching at room temperature. To investigate the SOT switching dynamics, the pulse current-induced SOT switching measurements were performed, and the anti-damping-like torque efficiency was quantified by measuring the harmonic Hall signals. We have observed a very reproducible deterministic SOT magnetization switching in Pt/TmIG devices with current density as low as 0.7×10^{11} A/m^2 under an external magnetic field of 5 mT.

Results and Discussion

TmIG films were grown on a GGG substrate using the on-axis RF magnetron sputtering technique at room temperature (Fig. 1b). Argon gas was introduced at a flow rate of 23 sccm after the optimization (see Supplemental Material S1). Post-annealing of the TmIG film was performed in an O_2 atmosphere at 800° C for 180 min to gain their crystallinity and magnetic properties. Pt film was deposited by dc-sputtering. Hall cross devices of TmIG/Pt heterostructures were fabricated by lithography and Ar^+ ion milling.

The crystal structure was examined by XRD patterns of 22 nm-thick TmIG film as shown in Fig. 1c. A Clear peak at 51.6° stemming from a strained TmIG (444) plane was observed in addition to the sharp peak from the GGG (444) plane. The peak of the TmIG (444) plane was the same as that observed in previous reports[6,23,34]. From these patterns, the out-of-plane lattice constant $a_{(111)}$ was 1.2275 nm.

To examine the crystal quality of a representative sample, a series of characterization was performed using an atomic force microscope (AFM) and a scanning transmission electron microscope (STEM). A flat surface with root-mean-square (RMS) roughness of 0.14 nm was observed (Fig. 1d). This excellent crystallinity of the TmIG film was also observed by a cross-sectional high-angle annular dark-field (HAADF) STEM image with atomic resolution and zone axis [110] (Fig. 1e). The STEM image disclosed that our TmIG film has the same crystal structure and orientation as the GGG (111)

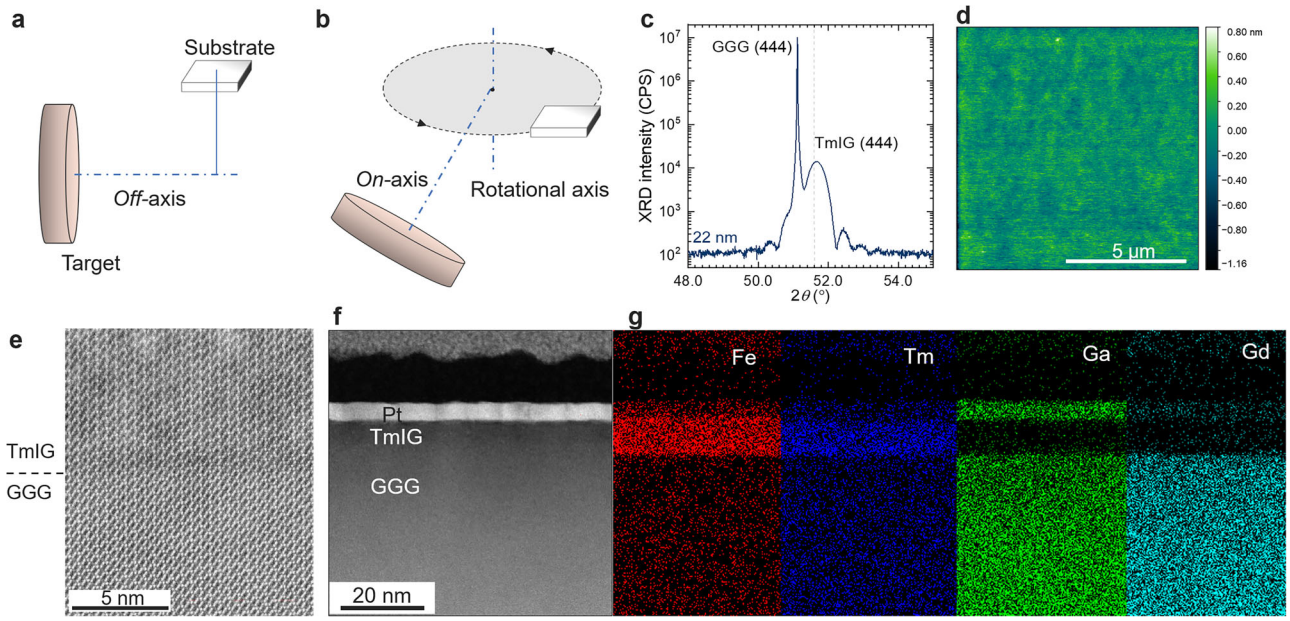

Fig. 1 | Growth of TmIG film and structural characterization. **a**, **b** Schematic diagram of off-axis (a) and on-axis sputtering (b). **c** XRD pattern of TmIG films fabricated by on-axis sputtering. **d** Surface morphology of a TmIG film observed by using atomic force microscope. **e** High-resolution scanning transmission electron microscopy of the interface between GGG substrate and TmIG film. **f**, **g** Scanning transmission electron microscope image and energy dispersive spectra of TmIG.

substrate. A sharp interface without atomic interdiffusion was confirmed by elemental mapping (Fig. 1e,f).

The magnetic properties were examined using the Magneto-optical Kerr effect (MOKE) and the superconducting quantum interference device (SQUID). MOKE signal under an out-of-plane field shows clear hysteresis expected from a PMA ferromagnet. From SQUID magnetometry, the signal measured in an out-of-plane magnetic field shows clear hysteresis, while the in-plane field scan shows the hard axis properties, indicating that the easy axis was normal to the film surface (Fig. 2a, b). The M_S is measured to be 100 kA/m, which is also in line with previous reports[34,36]. Figure 2c shows the magnetic field-dependent spin wave difference measured by Brillouin light scattering (BLS) using a 24 nm-thick TmIG film. Based on the clear Stokes peaks, the magnetic anisotropy was evaluated. The magnetic field dependent spin wave frequency curve is expressed by[37]:

$$f = \frac{\gamma}{2\pi}\sqrt{H(H + M_{\text{eff}})}, \quad (1)$$

where γ is gyromagnetic ratio, $M_{\text{eff}} = \mu_0 M_S - 2K_u/M_S$ is the effective magnetization. From the fitting, M_{eff} and K_u was evaluated as 64.3 mT and 9.5 kJ/m^3, respectively, which are in line with previous studies[34,38]. The signal of the anti-Stokes peaks was three orders smaller in amplitude than the Stokes peaks and unclear in our BLS measurement. Although non-zero Dzyaloshinskii-Moriya interaction (DMI) has been detected from TmIG[16], it was not quantified in our experiment because of the unclear signal of anti-Stokes peaks. DMI energy density is defined as the frequency difference between Stokes and anti-Stokes peaks in the BLS experiment. Hence, it is important that both Stokes and anti-Stokes peaks are well defined to extract DMI energy[37]. The characterization of DMI in the on-axis sputtered TmIG films will be investigated in future experiments.

Hall cross devices (Fig. 2d) were fabricated on TmIG/Pt heterostructures, with thicknesses of 6 nm and 3 nm, respectively. First, the anomalous Hall effect (AHE) was examined by applying a charge current (in the x-direction) and measuring the transverse voltage (in the y-direction) while sweeping the z-directional external magnetic field. The AHE in Fig. 2e shows a clear rectangular hysteresis with a coercivity of 7 mT, showing perpendicular magnetic anisotropy of TmIG at room temperature. The AHE observed in our sample was identified to originate from spin Hall magnetoresistance (more details in Supplemental Material S2). The bias current dependence of AHE was measured to estimate R_{AHE} to be 5.52 mΩ from the linear fitting (Fig. 2f).

Current-induced spin-orbit torque magnetization switching

Considering the application potential of the TmIG/Pt system for various spin-orbitronic devices, current-induced magnetization switching is very important, which was measured with a pulse current, as shown in Fig. 3a. We observed the reproducible deterministic SOT switching of the TmIG/Pt device at room temperature (Fig. 3b). In the presence of an external field in x-direction and a charge current, the magnetization is switched from the $-z$ direction to the $+z$ direction. The switching direction is opposite when we

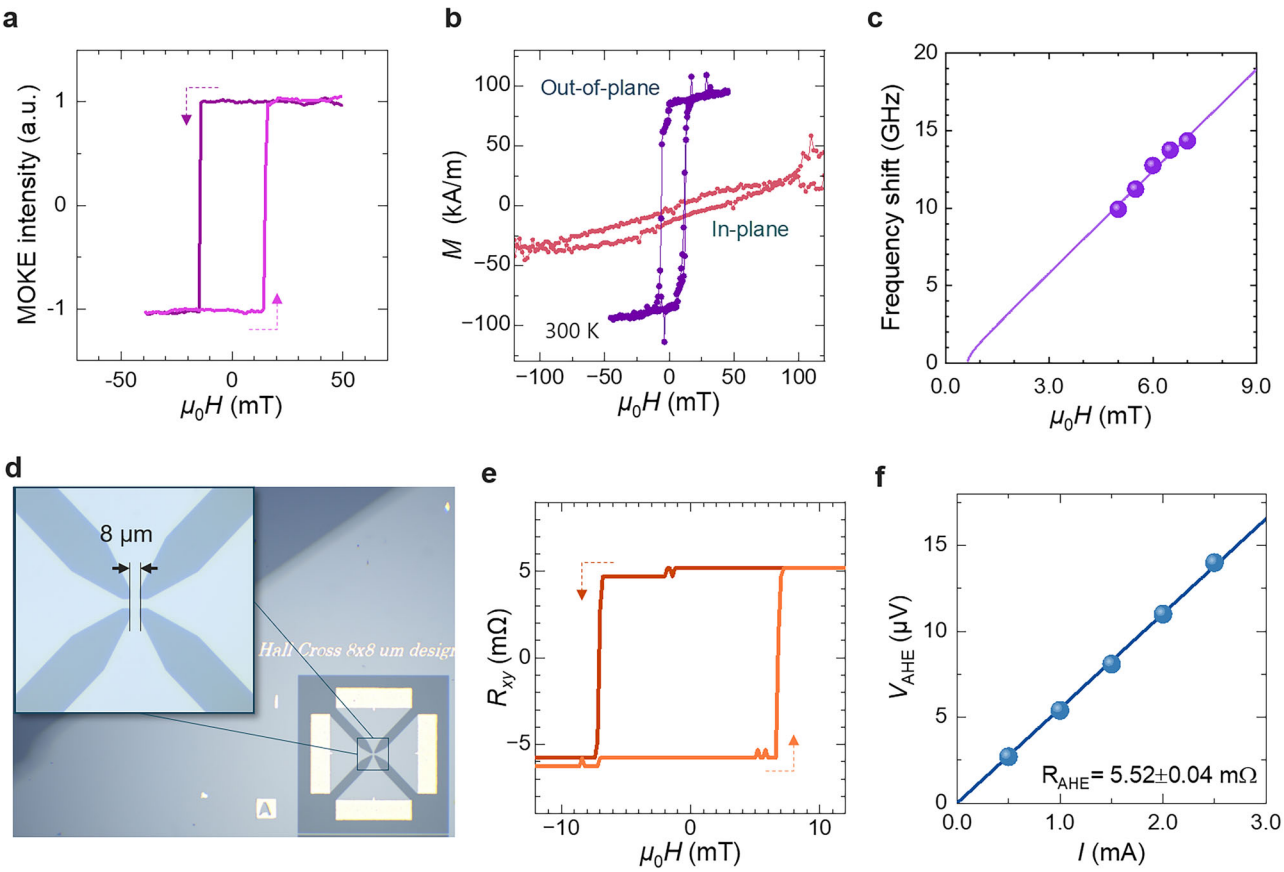

Fig. 2 | Magnetic characterization of TmIG film and TmIG/Pt heterostructures. **a** Results of magneto-optic Kerr effect (MOKE) measured under an out-of-plane magnetic field. The light and dark violet colors represent the positive and negative sweeps, respectively. **b** Results of magnetometry measured at 300 K for in-plane and out-of-plane. **c** The magnetic field dependence of spin wave frequency measured by Brillouin light scattering. The solid symbols and the line represent the experimental result and the fitting line by Eq. (1), respectively. **d** Optical image of TmIG/Pt Hall cross devices patterned with photolithography. The inset shows a magnified view of the Hall cross structure. **e** Anomalous Hall effect measured at room temperature for a TmIG/Pt heterostructure with a bias current of 1 mA after the subtraction of the ordinary Hall effect component. **f** Bias dependence of the anomalous Hall signals where $V_{\text{AHE}} = (V_{xy(+M\text{sat})} - V_{xy(-M\text{sat})})/2$. $V_{xy(+M\text{sat})}$ is the transverse voltage at saturation in the positive field and $V_{xy(-M\text{sat})}$ in the negative field. The solid symbols and the line represent the experimental results and linear fitting, respectively.

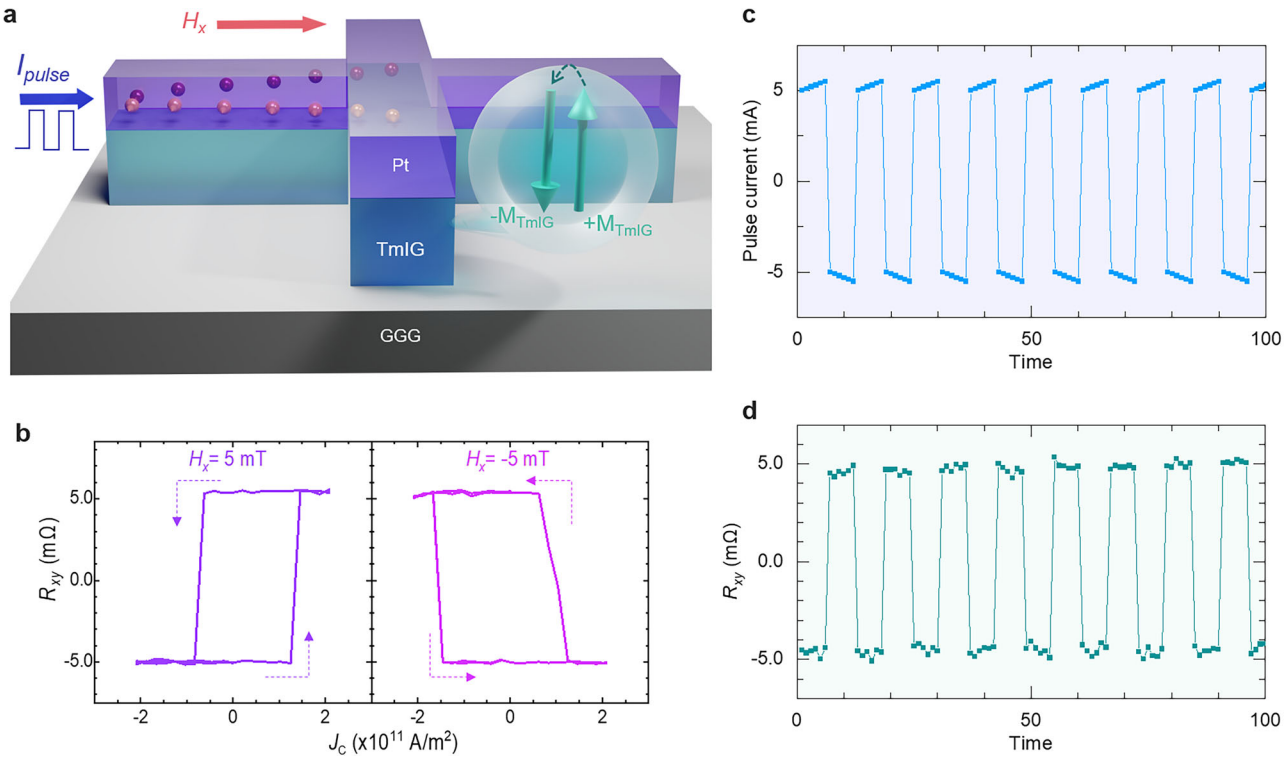

Fig. 3 | Current-induced spin-orbit torque magnetization switching in TmIG/Pt Hall devices. a Schematic diagram of switching measurements performed on TmIG/Pt heterostructures. A current pulse is applied to Pt along the x-axis, which generates a spin current through SHE along the z-axis, with spins oriented in the y-direction. An external magnetic field is also applied in the current direction to assist in magnetization switching. **b** Current-induced magnetization switching loops for TmIG/Pt heterostructures under external fields of + 5 and −5 mT. **c, d** Spin-orbit torque magnetization switching. The magnitude of consecutive applications of the 50 μs-width-pulse currents was from −5.5 to −5.0 mA in the negative polarity and from 5.0 mA to 5.5 mA in the positive polarity. The switching experiments were performed under an in-plane field of -5 mT (**c**). The Hall voltage was measured and plotted by applying 0.5 mA, 100 ms after each pulse current application (**d**).

reverse the external field direction, which agrees with SOT-driven magnetization switching. The critical current density (J_{sw}) was in the range of 0.7 to 1.5 × 10^{11} A/m^2. The asymmetry of the switching curve is sometimes observed in the SOT switching experiment. A possible reason is the x-component of the applied magnetic field, which has been discussed in ref. 39. The in-plane field as low as 5 mT was enough for breaking the rotational symmetry and observation of SOT switching. Robust and deterministic switching by pulse current was observed by applying consecutive pulse currents. The magnitude of the pulse current was in the range of +5.0 mA to +5.5 mA for the positive polarity and from -5.5 mA to -5.0 mA for the negative polarity, as shown in Fig. 3c. The polarity of the 50 μs-width-pulse current switches the anomalous Hall voltage, which was measured by applying a 0.5 mA for sensing (Fig. 3d).

Estimation of spin-orbit torque fields by second harmonic Hall measurements

The second harmonic measurement of the Hall voltage is a powerful tool for evaluating the SOT acting on perpendicularly magnetized magnetic films. We carried out a series of second-harmonic Hall measurements to extract the effective spin Hall angle in our device. The in-plane field scan was carried out to evaluate the damping-like torque generated by the spin Hall effect in Pt and acting on TmIG. The second harmonic signal $V_{2\omega}$ is expressed as the following[23]:

$$V_{2\omega}^{\phi=90^\circ} = \left(V_H^{\mathrm{AHE,SMR}} - 2V_H^{\mathrm{SMR}}\cos\theta\sin 2\phi\right)\frac{d\cos\theta}{dH}\frac{H_{FL}}{\sin(\theta_H-\theta)} + 2V_H^{\mathrm{SMR}}\sin^2\theta\cos 2\phi\frac{H_{DL}}{H\sin\theta_H} \quad (2)$$

where H, θ_H and ϕ are the magnitude, and the zenith and azimuth angles of the external magnetic field, respectively. θ is the zenith angle of the magnetic moment of TmIG (see Fig. 4a). V_H^{SMR} and $V_H^{\mathrm{AHE,SMR}}$ are the measured voltages stemming from spin Hall magnetoresistance (SMR) and the SMR-induced anomalous Hall effect, respectively. H_{FL} and H_{DL} are the field-like and the damping-like torque induced by spin-orbital torque. Since $V_H^{\mathrm{SMR}} \gg V_H^{\mathrm{AHE,SMR}}$ (see Supplemental Material S2), the second term is dominant to the total signal, Eq. (2) will be further reduced to

$$V_{2\omega}^{\phi=90^\circ} = 2V_H^{\mathrm{SMR}}\sin^2\theta\frac{H_{DL}}{H\sin\theta_H} \quad (3)$$

The first harmonic in-plane field scan for 0.5, 1.0, and 1.5 mA is shown in Fig. 4b. To estimate the damping-like SOT, $V_{2\omega}$ versus a function of $(2V_H^{SMR}\sin^2\theta)/(H\sin\theta_H)$ was plotted as shown in Fig. 4c. Following Eq. (3), the linear fitting was performed, and the slope yielded an effective damping-like field, H_{DL}. Then, the current density J_C dependence of H_{DL} was plotted as shown in Fig. 4d. The effective spin Hall angle $\theta_{\mathrm{SHE}}^{\mathrm{DL}}$ was evaluated based on the equation[23,29,40]:

$$\theta_{\mathrm{SHE}}^{\mathrm{DL}} = \left(\frac{2e}{\hbar}\right)\left(\frac{H_{DL}}{J_C}\right)M_S t_{FM}, \quad (4)$$

where e is an elementary charge, $\hbar$ is the reduced Planck constant, M_S is the saturation magnetization, and t_{FM} is the thickness of TmIG. The $\theta_{\mathrm{SHE}}^{\mathrm{DL}}$ of the TmIG/Pt sample was 0.030.

To examine the effects of growth conditions and energetic anion irradiation on TmIG film, the $\theta_{\mathrm{SHE}}^{\mathrm{DL}}$ and J_{sw} in the TmIG/Pt system fabricated by different methods in the literature are compared in Table 1. Although some variation can be seen, no remarkable differences are found compared to those reported in the previous research using laser ablation and off-axis sputtering techniques. Some variations in $\theta_{\mathrm{SH}}^{\mathrm{DL}}$ and J_{sw} compared to the literature can be attributed to the thickness of TmIG,

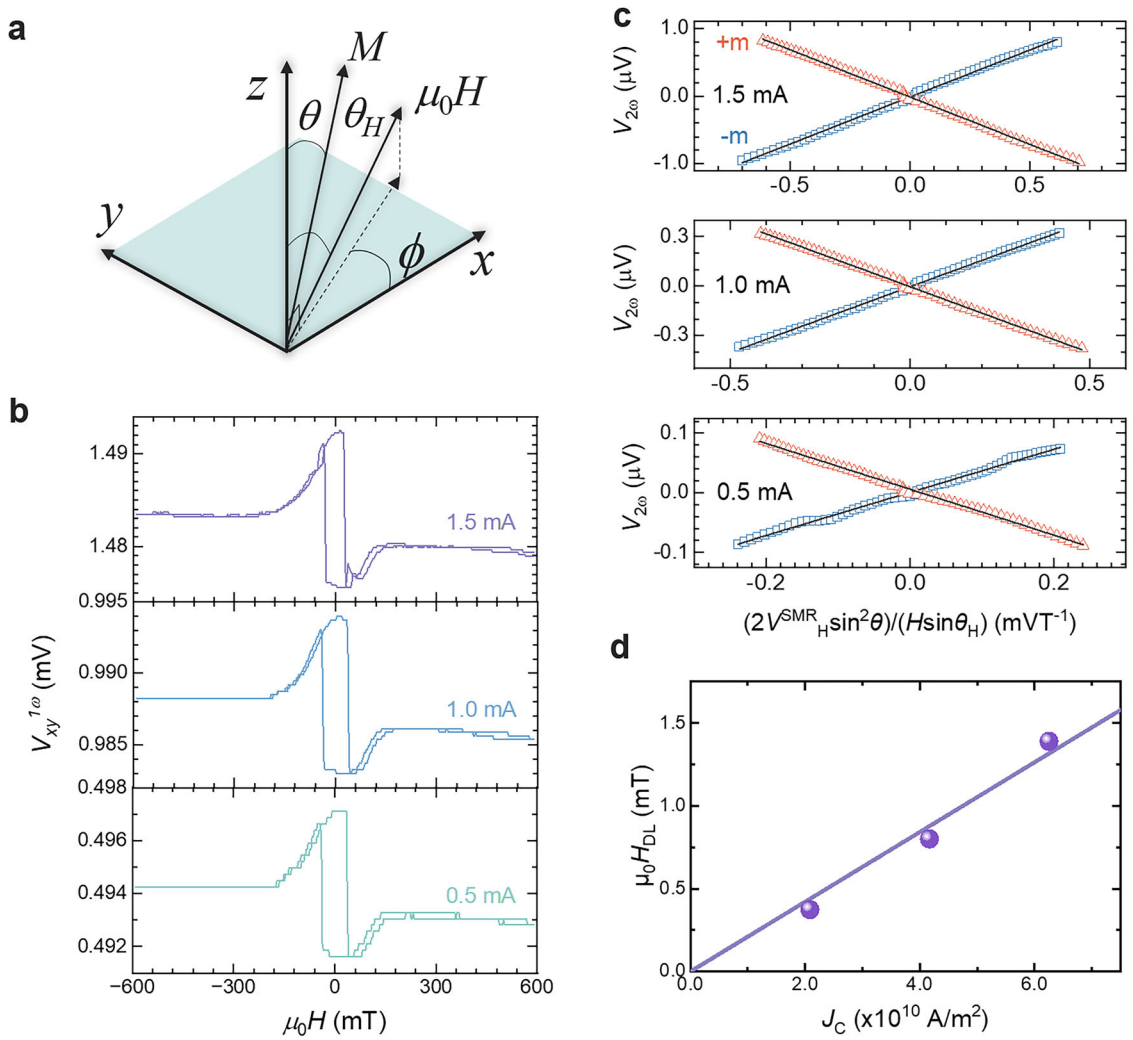

Fig. 4 | Second harmonic Hall measurements in TmIG/Pt Hall devices. **a** Schematic diagram indicating the angular parameters used for the analysis of the second harmonic signal. **b** In-plane field dependence of first harmonic Hall voltage with different current biases. **c** Linear fitting of the second harmonic Hall signals based on Eq. (3). **d** Current density dependence of the damping-like torque measured by the second harmonic Hall voltages.

Table 1 | List of spin-orbit torque efficiency measured in Pt/TmIG systems

Heterostructure (thickness in nm)	θ_{SHE}^{DL} (%)	J_{sw} (×10^{11} A/m^2)	$\mu_o H_x$(mT)	Growth	Method	Ref.
Pt(3)/TmIG(6)/GGG	3.0	0.7~1.5	5	Magnetron sputtering	2f-HE	This study
Pt(5)/TmIG(8)/GGG	1.5~2	1.7	50	PLD	2f-HE	23
Pt(4)/TmIG(9.6)/GGG	3	0.6	3.5	PLD	2f-HE	40
Pt(3.2)/TmIG(9)/GGG	8	0.25	0.5	Off-axis sputtering	2f-HE	36
CuO_x(3)/Pt(1)/TmIG(6.5)/GGG	1	1.7	2.5	PLD	χ, β-scan	32

2f-HE: second harmonic measurement of the Hall effect at a low magnetic field.
β-scan: angle dependence of the spin Hall magnetoresistance measurement.
χ: shift in the hysterisis loop with a bias current under a quadrapole magnetic field.

the quality of Pt film, and the interface between TmIG and Pt, as no significant difference in the magnetic properties of on-axis sputtered TmIG films could be observed.

The critical current density depends on the efficiency of the SOT and the volume of the magnet. In the TmIG/Pt system, all the charge current flows in the Pt. Part of the charge current is converted into a spin current at a conversion rate, modulated by the effective spin Hall angle. The spins accumulate at the interface of TmIG/Pt and exert torque on the magnetic moment of TmIG[23]. The magnetization is detected via the anomalous Hall effect due to the spin Hall magnetoresistance at room temperature, and due to the exchange coupling between *d*-orbitals of the Fe^{3+} ions in TmIG and the Pt[41] at the interface of TmIG and Pt. Thus, the quality of this interface is crucial to the performance of the SOT. The thickness of the magnetic film is important because it determines the volume of the magnet or the number of

spins to be flipped at the same current density seen from the formula of J_{SW}[4]:

$$J_{SW} = \frac{2et_{FM}D}{\hbar\theta_{SH}^{DL}\Delta}, \quad (5)$$

where t_{FM} is the FM thickness, D is the DMI energy, and Δ is the domain wall width. The thickness of the Pt is also important because it influences the magnitude of the spins accumulated at the interface of TmIG and Pt via the current density and the spin-diffusion process along the thickness direction.

The effective spin Hall angle θ_{SHE}^{DL} of 3.0% and J_{sw} of 0.7 to 1.5×10^{11} A/m^2 are comparable to those reported in the previous research using laser ablation and off-axis sputtering techniques. Therefore, no significant detrimental effects could be observed from the energetic irradiation due to the on-axis sputtering technique used for TmIG growth.

Summary

In this study, we demonstrated the SOT magnetization switching of TmIG thin film grown by on-axis radio-frequency magnetron sputtering. We systematically investigated the effect of growth conditions on the structural and magnetic properties of TmIG films, where excellent crystallinity and perpendicular magnetic anisotropy were achieved. In the Pt/TmIG heterostructure Hall bar devices, deterministic SOT magnetization switching was observed at room temperature, with competitive spin Hall conductivity and critical current densities. Second harmonic Hall measurements were performed to quantify effective damping-like torque, which is as high as previous reports. Our results show the potential of on-axis magnetron sputtering for the fabrication of ferrimagnetic insulators with perpendicular magnetic anisotropy for spintronic memory applications.

Methods

Sample fabrication

TmIG film was fabricated on GGG substrate by using radio frequency (RF) magnetron sputtering with on-axis geometry[34,35]. The base pressure of the chamber was lower than 10^{-5} Pa. The flow rate of Ar gas was set to 23 sccm, and the pressure during deposition was 3.0 Pa. No substrate heating was used. Post-growth thermal annealing was carried out at 800°C in O_2 atmosphere. Pt film was sputtered using RF magnetron sputtering, and Hall cross devices were fabricated by photolithography followed by Ar^+ ion milling.

Characterization of structural and magnetic properties

The crystal structure of the TmIG film was evaluated by using X-ray diffraction (XRD). Magnetometry was performed using a superconducting quantum interference device (MPMS3, Quantum Design). Parts of the sample were picked by using the same FIB system, and scanning transmission electron microscopy and elemental mapping of the energy dispersion spectra were observed by using JEOL JEM-ARM200CF.

Electrical measurements

AHE, SOT switching, and 2nd Harmonic measurements were performed in a system with a magnetic field up to 0.7 Tesla. Harmonic Hall measurements were performed with a Lock-in SR830 to measure the first and second harmonic voltages with fixed frequency $\omega = 213.34$ Hz. All the transport measurements were carried out at room temperature.

Data availability

The data that support the findings of this study are available upon reasonable request.

Received: 27 December 2024; Accepted: 15 August 2025;
Published online: 10 October 2025

References

1. Puebla, J., Kim, J., Kondou, K. & Otani, Y. Spintronic devices for energy-efficient data storage and energy harvesting. *Commun. Mater.* **1**, 1 (2020).
2. Bhatti, S. et al. Spintronics based random access memory: a review. *Mater. Today* **20**, 530 (2017).
3. Shao, Q. et al. Roadmap of spin-orbit torques. *IEEE Trans. Magn.* **57**, 800439 (2021).
4. Caretta, L. & Avci, C. O. Domain walls speed up in insulating ferrimagnetic garnets. *APL Mater.* **12**, 011106 (2024).
5. Avci, C. O. Current-induced magnetization control in insulating ferrimagnetic garnets. *J. Phys. Soc. Jpn.* **90**, 081007 (2021).
6. Kubota, M. et al. Stress-induced perpendicular magnetization in epitaxial iron garnet thin films. *Appl. Phys. Express* **5**, 103002 (2012).
7. Ciubotariu, O., Semisalova, A., Lenz, K. & Albrecht, M. Strain-induced perpendicular magnetic anisotropy and Gilbert damping of $Tm_3Fe_5O_{12}$ thin films. *Sci. Rep.* **9**, 17474 (2019).
8. Fakhrul, T. et al. Damping and Interfacial Dzyaloshinskii–Moriya Interaction in Thulium Iron Garnet/Bismuth-Substituted Yttrium Iron Garnet Bilayers. *ACS Appl. Mater. Interfaces* **16**, 2489 (2024).
9. Ding, S. et al. Interfacial Dzyaloshinskii-Moriya interaction and chiral magnetic textures in a ferrimagnetic insulator. *Phys. Rev. B* **100**, 100406 (2019).
10. Fakhrul, T. et al. Influence of substrate on interfacial Dzyaloshinskii-Moriya interaction in epitaxial $Tm_3Fe_5O_{12}$ films. *Phys. Rev. B* **107**, 054421 (2023).
11. Ding, S. et al. Identifying the origin of the nonmonotonic thickness dependence of spin-orbit torque and interfacial Dzyaloshinskii-Moriya interaction in a ferrimagnetic insulator heterostructure. *Phys. Rev. B* **102**, 054425 (2020).
12. Shao, Q. et al. Topological Hall effect at above room temperature in heterostructures composed of a magnetic insulator and a heavy metal. *Nat. Electron.* **2**, 182 (2019).
13. Althammer, M. et al. Quantitative study of the spin Hall magnetoresistance in ferromagnetic insulator/normal metal hybrids. *Phys. Rev. B* **87**, 224401 (2013).
14. Marmion, S. R., Ali, M., McLaren, M., Williams, D. A. & Hickey, B. J. Temperature dependence of spin Hall magnetoresistance in thin YIG/Pt films. *Phys. Rev. B* **89**, 220404 (2014).
15. Vlietstra, N., Shan, J., Castel, V., Van Wees, B. J. & Ben Youssef, J. Spin-Hall magnetoresistance in platinum on yttrium iron garnet: Dependence on platinum thickness and in-plane/out-of-plane magnetization. *Phys. Rev. B* **87**, 184421 (2013).
16. Tang, C. et al. Anomalous Hall hysteresis in $Tm_3Fe_5O_{12}$/Pt with strain-induced perpendicular magnetic anisotropy. *Phys. Rev. B* **94**, 140403 (2016).
17. Ding, J. et al. Nanometer-Thick Yttrium Iron Garnet Films with Perpendicular Anisotropy and Low Damping. *Phys. Rev. Appl.* **14**, 014017 (2020).
18. Zhu, Z. et al. Low-temperature quantum correction to anisotropic magnetoresistance in $Tm_3Fe_5O_{12}$/Pt heterostructures. *Phys. Rev. B* **105**, 184428 (2022).
19. Wang, Y. et al. Observation of nonlinear planar Hall effect in magnetic-insulator–topological-insulator heterostructures. *Phys. Rev. B* **106**, 155408 (2022).
20. Yang, C.-Y. et al. Direct observation of proximity-induced magnetism and spin reorientation in topological insulator on a ferrimagnetic oxide. *Appl. Phys. Lett.* **114**, 082403 (2019).
21. Yang, S. R. et al. Evidence for exchange Dirac gap in magnetotransport of topological insulator–magnetic insulator heterostructures. *Phys. Rev. B* **100**, 045138 (2019).
22. Lan, S. et al. Observation of strong excitonic magneto-chiral anisotropy in twisted bilayer van der Waals crystals. *Nat. Commun.* **12**, 2088 (2021).

23. Avci, C. O. et al. Current-induced switching in a magnetic insulator. *Nat. Mater.* **16**, 309 (2017).
24. Li, T. et al. Field-free magnetization switching with full scale in Pt/$Tm_3Fe_5O_{12}$ bilayer on vicinal substrate. *Appl. Phys. Express* **17**, 033003 (2024).
25. Bi, L. Z. et al. Field-free and energy-efficient switching of a ferrimagnetic insulator through orbital currents of copper. *Adv. Electron. Mater.* **10**, 2300627 (2024).
26. Bi, L.-Z. et al. Field-free switching of $Tm_3Fe_5O_{12}$ on miscut garnet substrates with entangled spin Hall magnetoresistance and anomalous Hall resistance. *Phys. Rev. B* **110**, 134415 (2024).
27. Ke, J. et al. Field-free switching and enhanced electrical detection of ferrimagnetic insulators through an intermediate ultrathin ferromagnetic metal layer. *Adv. Mater. Interfaces* **10**, 2300632 (2023).
28. Ke, J. et al. Intrinsic Magnetocrystalline Anisotropy Induced 3m-symmetry dependent field-free switching in epitaxial garnet films. *Phys. Rev. Lett.* **133**, 186703 (2024).
29. Husain, S. et al. Field-Free Switching of perpendicular magnetization in an ultrathin epitaxial magnetic insulator. *Nano Lett.* **24**, 2743 (2024).
30. Shao, Q. et al. Role of dimensional crossover on spin-orbit torque efficiency in magnetic insulator thin films. *Nat. Commun.* **9**, 3612 (2018).
31. Bai, H. et al. Large tunable perpendicular magnetic anisotropy in $Y_{3-x}Tm_xFe_5O_{12}$ (x= 0–3) Epitaxial Films With Minor Changes In Switching Current. *Phys. Rev. Appl.* **17**, 064023 (2022).
32. Ding, S. et al. Harnessing orbital-to-spin conversion of interfacial orbital currents for efficient spin-orbit torques. *Phys. Rev. Lett.* **125**, 177201 (2020).
33. Li, T. et al. Giant orbital-to-spin conversion for efficient current-induced magnetization switching of ferrimagnetic insulator. *Nano Lett.* **23**, 7174 (2023).
34. Agusutrisno, M. N. et al. On-axis sputtering fabrication of $Tm_3Fe_5O_{12}$ film with perpendicular magnetic anisotropy. *Thin Solid Films* **788**, 140176 (2024).
35. Agusutrisno, M. N. et al. Large-scale fabrication of thulium iron garnet film with perpendicular magnetic anisotropy using RF magnetron sputtering. *Jpn. J. Appl. Phys.* **63**, 07SP06 (2024).
36. Wu, C. N. et al. High-quality thulium iron garnet films with tunable perpendicular magnetic anisotropy by off-axis sputtering – correlation between magnetic properties and film strain. *Sci. Rep.* **8**, 11087 (2018).
37. Cho, J. et al. Thickness dependence of the interfacial Dzyaloshinskii–Moriya interaction in inversion symmetry broken systems. *Nat. Commun.* **6**, 7635 (2015).
38. Rosenberg, E. R. et al. Magnetic Properties And Growth-induced Anisotropy In Yttrium Thulium Iron Garnet Thin Films. *Adv. Electron. Mater.* **7**, 2100452 (2021).
39. Fan, W. et al. Asymmetric Spin-orbit-torque-induced Magnetization Switching With A Noncollinear In-plane Assisting Magnetic Field. *Phys. Rev. Appl.* **11**, 034018 (2019).
40. Avci, C. O. et al. Fast switching and signature of efficient domain wall motion driven by spin-orbit torques in a perpendicular anisotropy magnetic insulator/Pt bilayer. *Appl. Phys. Lett.* **111**, 072406 (2017).
41. Ding, S. et al. Anomalous Hall effect in magnetic insulator heterostructures: Contributions from spin-Hall and magnetic-proximity effects. *Phys. Rev. B* **104**, 224410 (2021).

Acknowledgements

This work was supported by JSPS KAKENHI Grant Number JP22K14292, JST ACT-X JPMJAX23KJ, JST ASPIRE JPMJAP2321, Japan International Cooperation Agency, Nippon Sheet Glass Foundation for Materials Science and Engineering, Murata Science and Education Foundation, and Scandinavia-Japan Sasakawa Foundation. N.Y. acknowledges Professor Takashi Kimura and Professor Naho Itagaki for providing access to their equipment. Parts of the experiments were carried out at the Low Temperature Center, the Center of Advanced Instrumental Analysis, and The Ultramicriscopy Research Center of Kyushu University. N.Y. acknowledges Mr. Tomoya Watanabe (R1 TECHNOLOGIES LLC.) for his support. S.P.D. acknowledges European Innovation Council (EIC) project 2DSPIN-TECH (No. 101135853).

Author contributions

R.N., N.Y., M.A., K.Y., Y.K. and H.Y. fabricated and measured the devices. R.N., N.Y., B.Z., S.K., I.C., S.L., C.Y., Y.K. and S.P.D. analyzed and interpreted the experimental data. R.N., N.Y., S.K. and S.P.D. wrote the manuscript with comments from all the authors. N.Y. and S.P.D. coordinated and supervised the project.

Funding

Open access funding provided by Chalmers University of Technology.

Competing interests

The authors declare no competing interests.

Additional information

Supplementary information The online version contains supplementary material available at https://doi.org/10.1038/s44306-025-00105-z.

Correspondence and requests for materials should be addressed to Naoto Yamashita or Saroj P. Dash.